일반총설

Scanning Probe Microscopy of Polymer Materials

K. J. Ihn and J. A. N. Zasadzinski

INTRODUCTION

In the 300 years of optical and 50 years of electron microscopy development, nothing has prepared us for the incredible imaging power and simplicity of scanning probe microscopy(SPM). The transmission electron microscope(TEM) and the scanning electron microscope(SEM) have served as very useful instruments to survey surface topology in wide variety of materials. However, both TEM and SEM have resolution limits in studying surface structures, and only give two dimensional images. In order to observe topology of polymer samples in TEM, shadowing methods using heavy metals such as Pt, Cr, and Au have been applied. The resolution of the shadow images is restricted by the particle sizes of shadow materials. The SEM is a powerful instrument, which directly gives images of the shape of materials. But the resolution of two dimensional SEM images is on the order of nanometers. A three-dimensional image of a surface with atomic resolution is only possible with a SPM, such as the scanning tunneling microscope(STM) and the atomic force microscope (AFM).

The capability of the SPM to probe the topography and electron structure of surfaces with atomic resolution makes it a powerful instrument for the study of surface chemistry. The STM[1] has the greatest proven resolution of any surface imaging technique ; for ideal samples the lateral resolution is about 0.1 nm and the vertical resolution is less than 0.01 nm.

The AFM was first developed by Binning, Quate and Gerber[2] in 1986 to image non-conductors. Here, instead of using an STM tip whose direction is normal to the surface of a sample, they positioned the tip in an almost parallel direction so that its sharp edge was just above the surface. The tip, acting as a cantilever, did exert a force on the sample in the same way that the STM tip does,

Kyo Jin Ihn

1982 한양대학교(공학사)
1986 한국과학기술원(공학석사)
1990 Kyoto University (공학박사)
현재 Visiting Scientist Materials Dapartment, University of California, Santa Barbara

Joseph A. N. Zasadzinski

1985 Ph. D in Chemical engineering, University of Minnesota
1986 Post-doctoral Position at AT&T Bell Laboratories
현재 Professor of Chemical Engineering and Materials Engineering, University of California, Santa Barbara

Materials Department, and Chemical & Nuclear Engineering
Department, University of California, Santa Barbara, California 93106, USA

except that now the minute deflections of the cantilever with its force-sensing edge were of importance. To measure the deflection of the cantilever, they used a second STM tip that could resolve cantilever deflections as small as 10^{-3} nm. Modern commercial AFM's detect the deflection of the cantilever by an optical lever, in which a laser beam is reflected off the cantilever tip into a segmented photodiode (Fig. 1(a)). The types of cantilevers most often used are either thin metallic wires or microfabricated silicon oxide (SiO_2) or silicon nitride (Si_3N_4) levers in rectangular or triangular structures.

AFM technology also has been extended to measure electrostatic[3] and magnetostatic interactions[4] as well as long-range van der Waals forces.[5~8] These forces are measured in noncontact mode of tip and sample. The first topic deals with monopoles, the second with dipoles, while the third requires a quantum mechanical treatment.[9]

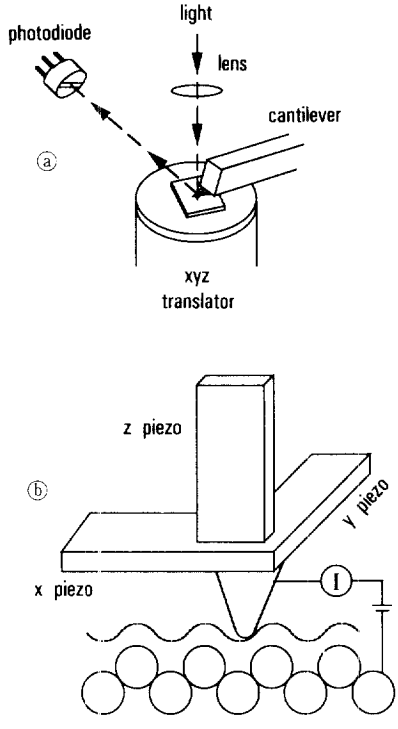

Fig. 1. Principles of AFM(a) and STM(b).

These forces and their derivatives can be as small as 10^{-12}N and 10^{-4}N/m, respectively, requiring resonance enhancement methods. An excellent review of these microscopies is listed in Ref. 10. These microscopic techniques measuring forces in noncontact and contact modes are included in the category of scanning force microscope (SFM).[10,11]

Now SPM is widely applied in a variety of research fields, e. g., semiconductor devices, clusters, metals, organic materials, biomaterials and polymers.[12] A number of research groups have begun interesting frontier studies of polymer materials. Until now many papers reporting SPM results have appeared in the rapid publishing journals. This trend directly reflects the rapid propagation and importance of SPM usage in polymer science. The application of the SPM is not limited to high resolution atomic images of polymer surfaces, but also have been extended to crystal structure analysis, nucleation, crystal growth structure and mechanism, deposition, adsorption, etc.[12] The SPM is only a few years old, however, with the abundance of work that has already approved, one can tell that SPM has a great potential in providing new knowledge about polymer and other materials.

This review is intended to give a basic understanding of SPM and its possible applications for polymer research. We will briefly introduce the principles of STM and AFM operation, and summarize several examples of STM and AFM studies on polymers and other materials. We will also discuss possible artifacts and other problems in using SPM.

Operating Principles of Scanning Probe Microscopes

Principle of STM : Classically, at room temperature, the electrons in the metal tip of STM do not have sufficient energy to leave the metal and enter the vacuum gap between the tip and a conductive sample. However, there is a small, but finite probability, that an electron wave can tunnel through the vacuum barrier into a second metal, if the separation between the two metal surfaces is small

enough. Solutions of the Schrödinger equation[13] show that the tunneling current, T, through the vacuum gap is proportional to :

$$T \propto \exp -\{[\frac{2m\pi^2}{h^2}(V-E)]^{1/2} S\}$$

S is the gap separation, m is the mass of the electron, and h is Planck's constant. Clearly, there is a non-zero probability that an electron can tunnel from the tip through the vacuum gap and appear in the other metal. This exponential dependence of tunneling current on separation is what makes the STM work so well. In practice, a bias voltage of a few millivolts to a few volts is applied between the tip and the sample, and the tunneling current is usually a few tenths of a nA.

To make best use of the unique properties of the tunneling current, it is necessary to be able to hold and position a metal probe within a nanometer or less of the sample surface while at the same time being able to raster this tip across the surface. In the original STM[14] this was accomplished with three, independently controlled, piezoelectric transducers of lead titanate/lead zirconate ceramic fixed in a tripod arrangement (Fig. 1(b)). The tip, which is usually a fine needle of tungsten, platinum/iridium alloy, or gold, is then mounted to the tripod. In modern, and in most commercial instruments, the tripod arrangement has been replaced by a single, cylindrical piezoelectric tube to which the tunneling tip is attached.[15] The electrodes on the outside of the tube are divided into four segments on opposite sides of the tube that control the rastering direction. A single electrode on the inside of the tube controls the vertical direction. The tube scanner is significantly faster and more resistant to vibrations than the tripod arrangement. Single tube piezoelectric transducers with ranges less than a nanometer to more than 100 microns have been designed. Hence, the modern STM can now determine structural information from the atomic scale to the range that is visible with the optical microscope. In addition, a typical STM image takes only a few to tens of seconds to acquire.

When the STM is operated, a metal tip is brought close enough to the surface to be imaged that electrons begin to tunnel between the tip and the surface at a convenient operating voltage (2 mV-2 V). The tip is scanned over the surface while the tunneling current is measured. A feedback network changes the height of the tip to keep the tunneling current constant in the so-called "constant height mode" or the current is monitored at constant tip height in the "current height mode". In the more-commonly used constant current mode, if the current can be kept constant to 2%, then the gap between the surface and tip remains constant within 10^{-3} nm.[14] The image consists of a map of the tip height vs lateral position which results in a three-dimensional rendition of the scanned surface.

Principle of AFM : The AFM traces out contours of constant force (as oppose to the STM which traces out contour of constant electron density) by rastering a sharp tip across the sample surface. The AFM tip, which is suspended on a cantilever spring is pushed very gently against the surface to be imaged. As the tip is scanned across the surface, the cantilever is deflected by the variations in the surface contours (Fig. 1(a)). The deflection of the cantilever can be measured with electron tunneling, interferometry, or by an optical lever.[16] All that is required is an electrical signal that varies rapidly with the deflection. This signal is then sent to the same type of electronics used for a STM. A feedback loop controls the voltage to the vertical piezo element on which the cantilever is mounted so that the force is held constant as the tip is scanned across the surface of the sample with the horizontal piezo element. As in the STM, one scan is a plot of the voltage applied to the vertical piezo as a function of the raster position. An image is built of many scans, each slightly offsets from the previous one.

The resolution of the instrument is determined by the reliability and sensitivity of detecting the cantilever motion and the resonant frequency of

the cantilever. The optical lever AFM (Fig. 1(a)) amplifies the motion of the cantilever to produce a motion of the reflected beam at the detector that is greater by a factor of $2L/l$, where $L=4$ cm is the distance for the cantilever to the photodiode and $l=100$ μm is the length of the cantilever.[16] The factor of 800 is sufficient so that the instrument is not limited by the photodiode lateral sensitivity, but rather by sound and building vibrations. The microfabricated cantilevers are made from silicon oxide or silicon nitride and have resonant frequencies of the order 100 kHz, resulting in a noise level small enough to permit routine atomic resolution imaging of non-conducting solids and crystals.[16]

Development of New Tip Geometries

The sharpness of the tip, or more exactly, its radius of curvature, determines the lateral resolution of the STM or AFM, given state of the art piezoelectric transducers. The use of very blunt tips, readily made by conventional machining methods, with radii about 100 nm sufficed in the early years of STM. If tunneling occurred with equal probability from all points of this tip, the lateral resolution would be on the order of the tip radius, and the STM would not be much of a microscope. What actually happens is that on virtually every tip, naturally occurring protuberances project farther from the tip than other atoms. Hence, the actual radius for tunneling is of atomic dimensions. Currently, to avoid multiple active probes and to minimize vibration and adhesion, very sharp tips with apex radii significantly less than 100 nm have been prepared by electropolishing or other methods.[17,18] The need for sharp tips in microscopy arose in the context of the field electron emission microscope.[18] Tungsten has been used almost exclusively from the early stages to make the tips. Other metals, including Pt/Ir and some semiconductors were later used. Several books are available with collected technical procedures for making sharp tips. Many ways to produce sharp tips of various materials for microscopy have been devised. (1) Electrolytic (electrochemical) polishing/etching ; (2) chemical polishing/etching ; (3) ion milling ; (4) cathode sputtering ; (5) whisker growth ; (6) vapor, electro- or electron-beam deposited ; (7) flame polishing ; (8) mechanical shaping : (a) oil-stone hand polishing, (b) cutting, (c) machining, (d) fragmenting, (e) bashing ; (9) combinations of some of the above ; (10) others.[14,17,18]

Electrolytic methods are a major way in which STM tips are prepared. Fig. 2 shows one of the scheme to make a tip by an electrolytic method.[18] The electropolishing process can be monitored by eye or by optical microscope and stopped when the specimen region near the air-liquid interface has completely "necked-in" and a small piece below this region has fallen away (dropped-off). More detailed procedures are described in ref. 17, 18. For in situ characterization of electrode surfaces, a preparation method of glass and polymer coated STM tips that possess < 10 nm apex radii

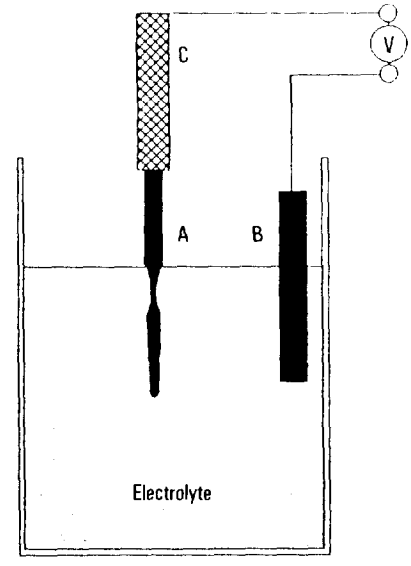

Fig. 2. Configuration of a simple electropolishing scheme. A is the specimen blank, B is the counter electrode, C is a mechanicallyheld clamp, and V is either AC or DC(with the specimen positive) voltage. (cited from ref. 18)

was reported by Heben et al..[19,20]

For the SFM, sharper tips, with a nominal radius of 10 nm, were recently developed by Park Scientific Inc. through a microfabrication process.[21] The tips are conical in shape, while conventional tips are pyramidal with nominal radii of about 40 nm (Fig. 3). The SFM with the new tip is reported to have significantly better resolution.

STM Studies on Polymer Materials

Most organic materials are extremely poor conductors of electricity. Hence the STM treats organic materials as if they were part of the potential barrier, if they are thin enough to tunnel through. In fact, there are many STM studies treating many non-conductive polymers in addition to conductive polymers.

Nucleation and Growth of Conductive Polymers : Many conductive polymers containing conjugated bonds are insoluble in common solvents, and this property has made structural characterization difficult. There are, however, several STM papers that have been successful in imaging the molecular structures of conductive polymers and the morphologies of the initial stage of polymerization and growth. This demonstrates that STM is suitable to test the structures of conductive polymers.

Yang et al.[22] observed typical microisland and strand structure in electrochemically deposited and doped polypyrrole that related to the nucleation and growth pattern, shown in Fig. 4. The conducting polymer films have a structure which gradually changes from an ordered crystalline array at the surface to an amorphous materials in the bulk. Yang et al.[23] observed a helical molecular structure for doped polythiophene, and found that STM measurements of the helical pitch and the diameter agreed quite well with X-ray measurements.

The STM study of Hecki and Smith[24] on electropolymerized glutaraldehyde having poor conductivity showed that it is possible to use STM as an instrument to form polymerized clusters on a nanometer scale and to investigate the process of polymerizing small organic monomeric molecules to oligomers. STM is more often used to study nucleation and growth mechanism of inorganic

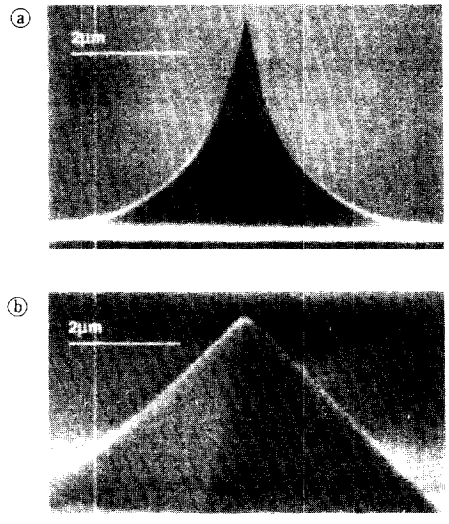

Fig. 3. SFM tips.(a) Conical shape tip, and (b) conventional pyramidal tip. The silicone cantilevers and integral probe tips are produced by microfabrication process.(cited from ref. 21)

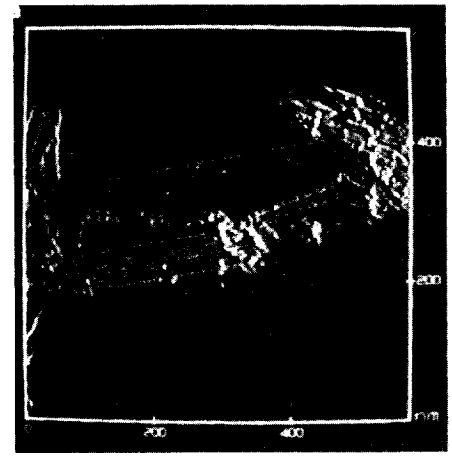

Fig. 4. Nucleation and growth pattern of polypyrrole doped by p-toluene sulfonate, consisting of polymer strands growing between the polymer islands.(cited from ref. 22)

materials, i.e., hydrogenated amorphous carbon films,[25] chemical deposited diamond films,[26] Pt,[27] Ag and Au films,[28~30] etc.

Electrochemically Deposited Polymers : In this section, we will introduce several examples of electrochemically deposited conductive polymers. The observations of fine structures were first made by STM. TEM does not usually give very good contrast because the polymers are not very ordered.

Morphologies of polyaniline electrochemically deposited onto a thermally evaporated gold electrode substrate were investigated by Jeon et al.[31] in the nucleation stages. They observed an increase in population of nuclei and homogeneous film by increasing the deposition time. They also reported interesting results of tunneling experiment of the fully doped polyaniline and the π-π^* gap was found to be 4 eV, in close agreement with optical adsorption microscopy. They showed that the tunneling conductance at the Fermi level was finite and changed spatially, suggesting that the observed results were consistent with metallic behavior based on a single polaron lattice model.

STM images were obtained by Caple et al.[32] from deposited thick films of polythiophene, poly(3-methylthiophene), and poly(3-bromothiophene), which were electrochemically deposited on a platinum substrate. They assumed that the sulfur atoms are involved in the tunneling process. Films of both chemically and electrochemically prepared poly(hydroxy-aniline) were imaged by Porter et al.[33] with the STM. Both types of films showed amorphous, island-like structures of average diameter 1 μm and height 10 nm and an abundance of free-standing polymer strands. The average diameter of the strands was approximately 2 nm, and the periodicity along the strands was approximately 3.15 nm and 2.95 nm, for chemically and electrochemically prepared strands, respectively. Coil or simple helical structure of strands was deduced from these dimensions. Oka and Takahashi[34] observed iodine doped poly(N-vinylcarbazol) deposited on 'highly oriented pyrolytic graphite' (graphite) and the size of the global shape of deposited polymer complex was compared with the shape of a random coil in free space.

Since a STM image may give atomic resolution, the obtained atomic image may be complementary to the structure analysis of unknown material. A structure analysis was done by Kempf et al.[35] for two conductive polymer systems ; poly(4-vinylpyridine) and poly(butadiene-b-4-vinylpyridine) with 7,7', 8,8'-tetracyanoquinodimethane (TCNQ) using X-ray diffraction, STM and FTIR. They found from this combined structure analysis experiments that the charge transfer complex formed between the pyridine group and the known electron acceptor, TCNQ, is the conductive element in these systems.

STM for Nonconductive Polymers : There are many reports on observations of non-conductive polymer molecules and other materials, such as nucleic acids,[36~38] proteins,[39~41] etc.[42~44] These observations unveiled many unknown structures of less-ordered polymers, that can be extended to develop an understanding of the phenomena of adsorption, adhesion and compatibility.

Yang et al.[45] observed poly(ethylene oxide) samples on graphite surface prepared by applying a drop of 0.1 wt.% ethanol solution. The images, showing individual monomer units, were consistent with the crystal structure analyzed by Tadokoro et. al., irrespective of molecular weight. From the analysis of the STM images they suggested single, double and multistranded helical structures. The proposed superhelical structure was also similar to those of polypyrrole and polythiophene.

Ultra-high molecular weight polyethylene(PE) precipitated from a 10^{-5} g/ml of xylene solution by rapid cooling on a mica sheet was examined by Reneker et al..[46] The top surface of a thin, conducting layer of evaporated Pt/C on a polymer revealed much the same information as was obtained by removing the Pt/C layer and examining it with a TEM. They could observe fine line structures with 0.75 nm spacing that is close to the molecular distance in(020) surface of PE. They could not explain the reason of this observation of nonconduc-

tive PE molecules from the shadowed sample. However, it is not strange that the image was taken from the uncovered region by shadowing materials and the gap was enough to allow the tunneling current to pass through.

Several nonconductive polymers such as PE,[47] phthalocyaninato-poly-siloxane (and a polydiacetylene),[48] and poly(1-butene)[49] deposited on graphite surface were imaged with the STM, but the contrast formation from insulating polymer chains in STM is still not understood. Fig. 5 shows a STM image of a melt drawn poly(1-butene) film. The measured interhelical distance of about 0.42 nm does not coincide with the expected value of about 0.6 nm. This was interpreted in two ways.[50] 1) The presence of the lattice has a dramatic influence on the packing or the molecular array. 2) The measured superstructure might be a purely electronic effect with the molecular helices originating from the interference between the graphite and the poly(10butene) film. This observation indicates possible artifacts of STM images, which will be discussed later.

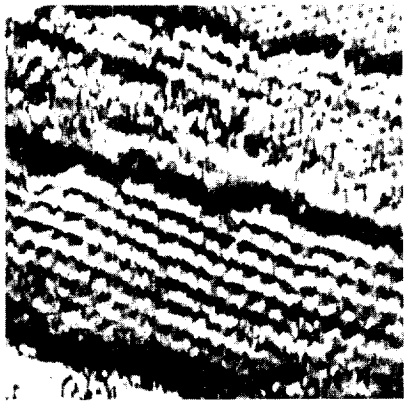

Fig. 5. High-resolution STM picture of a graphite surface covered with a poly(1-butene) film. In the lower right corner automatically resolved lattice of graphite is visible. The helical structure originating from the film filaments has a pitch height of ~0.38nm. The distance between the helices is measured to be 0.42 nm. Image size 7.5×9.2nm².(cited from ref. 49)

Application of STM : An interesting paper measuring the local piezoelectric activity[51,52] of a thin polymer film by STM was first reported by Birk et al..[51] A thin copolymer film of vinylidene fluoride and trifluoroethylene (60/40 mol %) with ca 1 μm thickness was prepared by a spin coating technique, and its piezoactivity was measured in the experimental setup shown in Fig. 6. They applied a slowly varying (20Hz) triangular driving voltage U_d to the electrodes as shown in Fig. 7, and measured directly the vibrational amplitude perpendicular to the sample surface. The measured local value of the piezoelectric constant d_{33} was -0.03 nm/V on the poled copolymer films, which is in good agreement with macroscopic observations on thicker films.[53] Again they found a typical hysteresis effect with saturation behavior for electrical field above 90 MV/m, when a slowly variable electrical field was applied to measure the field induced local piezoelectric surface motion.

Tunneling spectroscopy in the STM provides a

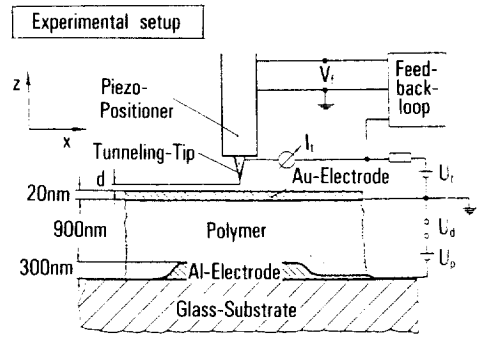

Fig. 6. Experimental setup for measuring the local piezoelectric activity using a scanning tunneling microscope : The polymer film is sandwiched between an Al-bottom electrode and a gold film as a top electrode. The tip of a STM is located just above the gold electrode(V_f = feedback voltage, U_t = bias voltage, and I_t = tunneling current). The feedback loop controls the z position of the tip. The voltage U_p can be used to pole the copolymer film or to switch its polarization into the reverse direction and U_d drives the film piezoelectrically.(cited from ref. 51)

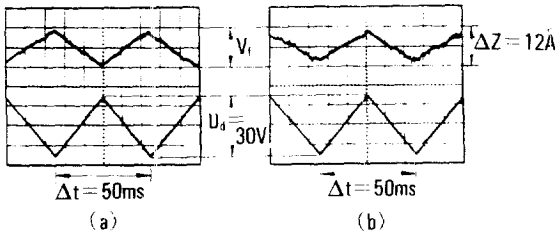

Fig. 7. The piezoelectric surface motion of a copolymer film as measured by STM in a constant current mode. The slowly varying triangular driving voltage U_d(lower trace) and the feedback voltage V_t(upper trace, typically 40mV) are plotted as function of time for (a) positive and for (b) negative polling. The absolute value of the surface amplitude Δz is driven from the calibration of the z piezopositioner.(cited from ref. 51)

direct measurement of local electronic properties with spatial resolution in the order of nanometers, which might be related to conduction mechanisms in polymers. Bonnell and Angelopoulos[54] characterized spatially localized electronic structure in polyaniline by STM. They determined variations of local electronic structures of fully and partially protonated emeraldine hydrochloride films. They found that two types of electronic structure predominate, a highly conductive metallic-like, and a less conductive semiconductive-like structure on length scales of tens of nanometers. They also found evidence for the existence of regions with a locally stable bipolaron configuration.

Another interesting application of STM is in microlithography[55~57] because the STM is capable of forming a low-voltage, submicron beam with extremely high current density. McCord and Pease[56] reported using a modified STM in microlithography. Poly(methyl methacrylate) films as a negative resist were exposed with the modified STM and the patterns were transferred into metal films using a liftoff technique. Even though the patterns were close to the highest resolution ever achieved with polymer resists on bulk substrates, they discussed, certain limitations that have to be overcome in this technique.

AFM Studies

The AFM has been developed more recently in 1986,[2] and AFM's have only started to be commercially distributed recently. Accordingly, only a few papers about AFM studies on polymer materials have been reported. Despite the short history of AFM, the enormous potential of this technique is obvious because the images are invariably superior in comparison with any other technique for studying the surface morphology of polymers. One of the merits of AFM is the visualization of non-conductive polymers and organic materials, which was impossible with the STM. If we broaden our investigations to other materials, especially to biomaterials, we can easily find that AFM is important because of its own exclusive merits. This will be discussed in the last section of the review.

The AFM is very compatible with a variety of environments, including liquids like water or saline. Operating the AFM with a sample and cantilever under water allows not only for more realistic environments, but for better control of the applied forces. The AFM is capable of imaging with a tracking force of about 2×10^{-9} N under water, which allows much softer surfaces to be imaged.[58] A fluid cell is shown in Fig. 8, which is used by Manne et al.[59] to study electrochemical adsorption and deposition of Cu on[111] surface of Au in situ.

Polyethylene Dendrites : One of the first AFM studies on commercial polymers appeared in 1990 by Patil et al.[60] for dendrite crystals of PE. They tried to evaluate the ability of the AFM to analyze

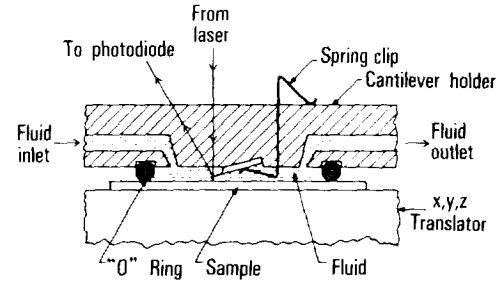

Fig. 8. Cross section of a fluid cell for AFM.(cited from ref. 59)

morphological features that are well known from TEM. Fig. 9(a) shows a region near apices of a typical dendritic crystal. The double rows of growth spirals described by Geil and Reneker[61] run from each of two apices of the basal lamella in the upper left part of the figure.

Fig. 9(b) and (c) show the capability of the AFM to measure the height of the sample, which is difficult to determine quantitatively with the TEM. The height of spiral terraces along the line in Fig. 9(b) is plotted in Fig. 9(c). The height difference between the two points of the arrowheads was 15.2 nm. All of the lamellae measured were close to 15 nm thick, which is a typical characteristic of lamellar crystals. Fig. 9(c) suggests an important artifact of AFM. The authors used a square-pyramid formed silicone nitride crystal tip. This shape has appeared in the edge of each lamella, which should have been normal to the basal plane. This means that their data were convoluted due to the shape of the tip. Clearly, this effect must be taken into account in the interpretation of the AFM data.

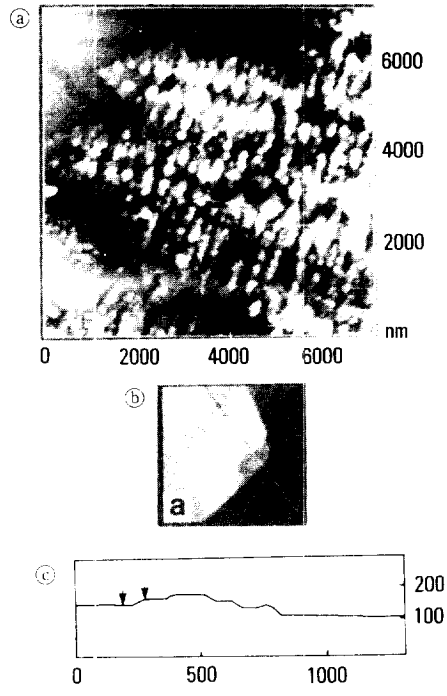

Fig. 9. (a) Dendritic crystal of polyethylene on mica grown from a 0.1% xylene solution. (b) Spiral terraces near an apex of a basal lamella. The edge of the area shown is 1.2mm long. (b) Cross section plot of a spiral terrace along the line shown in (a). (42) : (cited from ref. 60)

Cycloalkanes as a Model of Chain Folding in Polyethylene : A series of AFM studies on polymer samples has been reported by the Magonov and Cantow group on cold-extruded PE,[62] normal- and cyclic- alkanes,[63] 2,4-hexadiynylene bis(p-fluorobenzenesulfonate) and its monomer crystal,[64] polypropylene,[65] and polytetrafluoroethylene and polycarbonate.[66] They confirmed the molecular structure of various polymers using AFM. Amongst their interesting results are AFM images of cycloalkanes, [63] the structures of which have been regarded as a model of chain-folding in PE.[67] The four methylene units in a trans zigzag conformation form the (001) surface of cyclohexatriacontane in a regular fashion as shown in Fig. 10(a), which was computer simulated by SCHAKAL, a molecular graphics program.[68] The corresponding AFM image of cyclohexatriacontane is shown in Fig. 10(b). From the figure we can confirm again the regular-sharp folding structure in the cycloalkane. In the near future it is expected that AFM study can image chain folding structures in PE, which has been a long lasting puzzle in polymer physics.

Polypropylene : Isotactic-polypropylene(i-PP) is one of the more common polymeric materials. It shows three crystalline modifications. The recently found γ-phase has an unique structure, in which the polymer chains are not packed parallel along a single direction in the crystal structure ; a structure not yet found in any other polymer crystals.[69] Lotz et al.[65] performed AFM studies on the α-phase of i-PP, and successfully revealed the contact plane of the polymer when crystallized on the surface of benzoic acid. Fig. 11(a) shows the two unit cells of i-PP projected along the c-axis. Electron diffraction experiments revealed that (010) plane is parallel to the benzoic substrate surface.

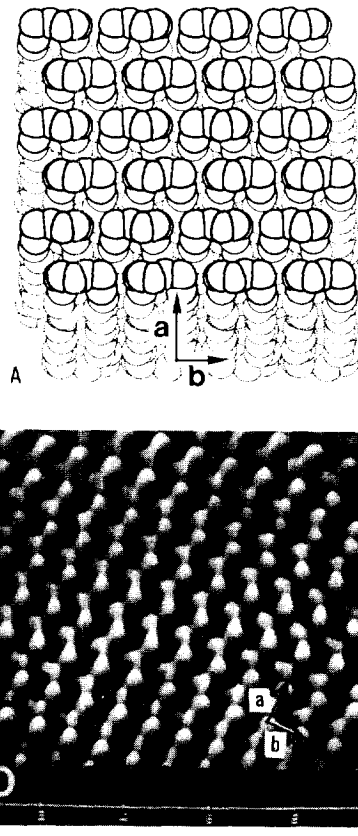

Fig. 10. (a) Drawing and (b) three dimensional AFM image of (001) plane of cyclohexatriacontane, $(CH_2)_{36}$ (cited from ref. 63)

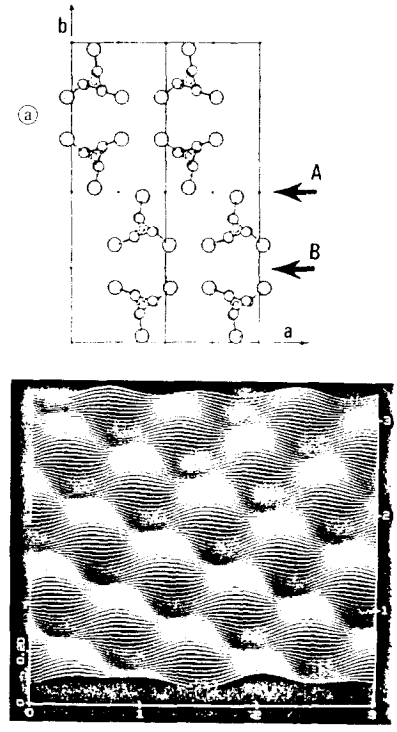

Fig. 11. (a) Two unit cells of α-phase i-PP. The large circles show methyl group, and small circles show main carbon atoms, which are packed in 3/1 helix. (b) AFM image of i-PP contacted with benzoic acid crystal surface.(cited from ref. 65)

In this case two (040) contact planes are possible, as marked in Fig. 11(a) with letters A and B. And the corresponding b-axis projections are again shown in Fig. 12(a) and (b), respectively. The high-resolution AFM image of Fig. 11(b) showed a mirror image of Fig. 12(a). Therefore, they could define that the surface that appeared in Fig. 12(a) is the exposed contact plane, and that the helix is right handed.

Applications of AFM for Quantitative Measurements : AFM can also be applied to test the quality of surface and thickness measurements as well as to obtain high-resolution images. This section will introduce briefly the present work in our laboratories regarding polytetrafluoroethylene (PTFE) layers.[69] The preliminary results illustrate an example of AFM application to a quantitative measurement of thin polymer films.

Wittmann and Smith[70] reported that PTFE layers deposited on glass surfaces by a rubbing method are ordered like a single crystal. They also found that the layers can be used as a substrate to orient many other crystalline polymers, liquid crystals, and small organic and inorganic materials. Magonov et al.[66] and Hansma et al.[71] have already, independently examined these layers, using AFM. Our present work using AFM is aiming at finding the influence of processing parameters, such as temperature, pressure, deposition speed,[72] on the continuity and thickness of the samples. Fig. 13(a), (b) and (c) show an AFM image of PTFE layer,

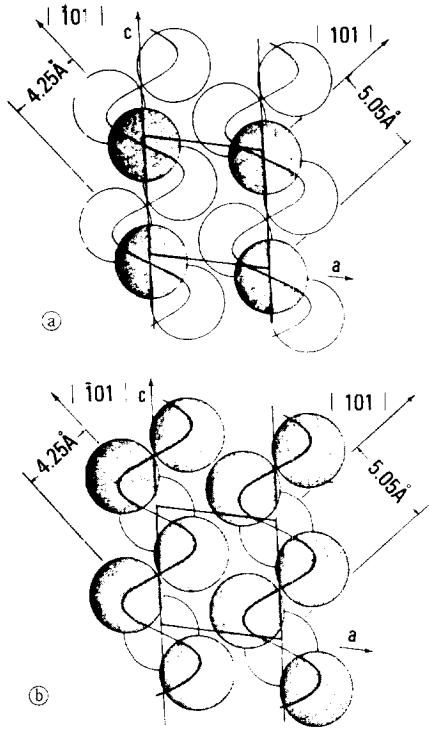

Fig. 12. Two possible surfaces of (040) contact plane of i-PP. One (a) and two (b) CH_3 groups are exposed on the surface(darker circles).(cited from ref. 65)

the height variation along the line in (a), and density of heights. From Fig. 13(b) and (c) we could compare the continuity and average thickness of the PTFE layers. We have found that the thickness ranges from 20~150 nm, and that it increases with increasing temperature and pressure applied during deposition. More continuous films were obtained at slower deposition speeds.

Modification of SPM and its Samples

In order to improve the performance of STM and AFM, the ordinary STM or AFM, which only give structural informations, have been modified.[51, 52, 54~57, 73, 74] And the STM or AFM sometimes combined with other instruments, such as SEM, TEM and optical microscope.[75,76] These combined instruments are able to both take images and measure physical properties simultaneously.

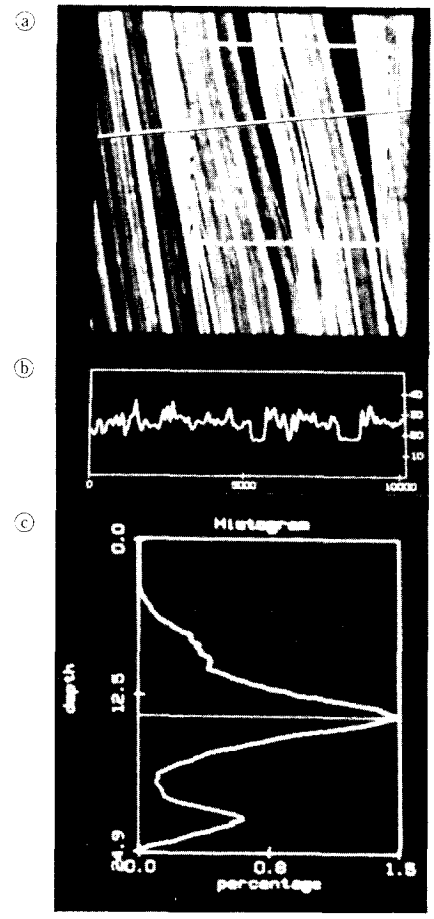

Fig. 13. (a) AFM image of PTFE thin film produced onto a glass surface by rubbing a PTFE rod across. (b) Height variation along the line in (a). (c) Histogram showing the height distribution from the square area in (a).(cited from ref. 69)

Some sensitive samples are difficult to image under normal conditions. To make contamination free samples and to make observations at that condition, the SPM has sometimes been carried out under ultra-high vacuum conditions.[77] For biological samples, lateral resolution of AFM is often limited to nanometer levels, due primarily to the AFM tip and sample interactions. Several approaches to immobilize and stabilize softer flexible macromolecules for AFM has been examined, notably,

tethering, coating, and freezing.[78] Although each approach has its advantages and disadvantages, rapid freezing techniques have been the special advantage for avoiding chemical perturbation and minimizing physical disruption of the sample.[78,79] Fisher et al.[78] reported a AFM technique operating at cryogenic temperatures (143°K), which has a potential to image frozen biomolecules at a high-resolution.

Most SPM samples are normally observed without further modification by mounting on to substrates, such as graphite, Au, mica, Si, etc. Sometimes preparing the samples by rapid-cooling is important for the materials changing the phases with temperature variation, such as liquid crystals, micells, etc. Traditionally the images of liquid crystalline materials in a particular phase have been taken by TEM using a freeze-fracture replication method. Zasadzinski et al.[80~82] have compared the TEM and STM images of freeze-fractured replica samples of a ripple phase. They could obtain much more informations about the structure from the three-dimensional STM images, which also have a higher resolution.

Discussion and Suggestions for Further Work

The examples of the studies using STM and AFM mentioned above allow us to get the impression of current usage of these techniques. The majority of the reports are only confirming the conformation of known structures, and, perhaps, this may be the first task for this new experimental tool. In addition, however, potential application of SPM has been demonstrated, not only for pure academic interest but also for applied creative works.

Expectations for SPM's : STM and AFM can readily give high-resolution images of atomic or molecular structures. These high resolution images are especially convenient to examine defect structures of materials, which sometimes lead to poor mechanical properties. Also, STM and AFM may become adequate tools to study modified surfaces, such as, plasma-polymerization, adhesion, etc. Their imaging processes are non-destructive, thus SPM can be applied to survey many dynamic shape changes of specimens, for example, sorption, desorption and transportation of materials, nucleation and growth of crystals, and growth of polymers onto polymerization catalysts, etc.

Defects and Artifacts of SPM Images : There exist some limits on the performance of SPM for the structure analysis of unknown samples, because it is sometimes difficult to interpret the obtained data without any knowledge about the structure of the samples examined. Generally no single instrument should be used to determine structure, however, and the information obtained from SPM images can be crucial to a complete structural analysis. This is especially important for less-ordered complex materials, such as LB membranes,[83,84] charge-transfer complex polymers,[35] since these materials usually yield limited information in conventional analysis instruments.

One has to carefully interpret SPM data because of new artifacts associated with the technique. There are several papers reporting artifacts of SPM images.[50,69,85~87] Even if a SPM is calibrated, artifacts may arise when the scanning area of interest is tilted with respect to the xy-scanning plane of the tip. When we observed the PTFE samples shown in Fig. 13(a) in a high magnification, for example, the surface of PTFE layer was tilted by 45° or even more, but still gave molecular resolution.[69] Consequently we observed significant artificial reduction of molecular spacings from the tilted area.

Artifacts can be created by the tip, substrate, and the interaction between them.[50,85~87] Leung and Goh[86] reported, for example, an interaction between the tip of an AFM and polystyrene molecules. They found that the tip produces a persistent deformation on the film. Some of the polymer molecules were pulled up by the tip, and artificial periodic nanometer-size structures were observed.

Merits of SPM in Comparison with TEM : STM or AFM are much more compatible with many modified or un-modified surfaces than the TEM, so

less sample alteration is necessary. TEM samples have to be thin (normally<0.1 μm) enough to allow transmission of the electron beam. Both the STM and the AFM can operate at room temperature and pressure, and even under fluids, including water. TEM is operated in a high vacuum (10^{-7} torr). Both instruments are much less destructive to samples than the TEM because the energy input, a few mV vs hundreds of kV, is much less. The energy in the electron beam of a conventional TEM is sufficient to break most organic chemical bonds, and often causes gross structural rearrangements on the time scales required for normal imaging. Also, electron micrographs are two-dimensional projections, as opposed to the three-dimensional topographies provided by the STM and AFM. Hence, even at their present embryonic level of development, the STM and AFM can provide a wealth of new information. The commercial availability of the STM and AFM at relatively modest prices will also spur new workers apply these extraordinary methods to their materials. Still, the scientist who hopes for molecular and eventually atomic resolution images of many materials faces many challenges before this goal can be reached. However, it is important to remember that the SPM is still in the early stages of development, and that many sample preparation techniques need to be optimized before these instruments can fully realize their potential.

Acknowledgments : K. J. I. is very grateful to Dr. T. W. Son in KIST for his encouragement of this work. K. J. I. is deeply indebted to Prof. P. Smith and Dr. F. Motamedi for helpful comments and fruitful discussions. We appreciate to the authors and publishers for the permission of their figures to be referenced and reproduced. Financial supports were provided by National Science Foundation, Grant ≠ DMR 91-00033 (K. J. I.), and by the Office of Naval Research, Grant # N00014-90-J-1551, a Whitaker Foundation Biomedical Engineering Grant, and by a National Science Foundation Presidential Young Investigator Award # CBT 86-57444 (J. A. N. Z.).

REFERENCES

1. G. Binnig and H. Rogrer, *Helv. Phys. Acta*, **55**, 726 (1982).
2. G. Binnig, C. F. Quate, and Ch. Gerber, *Phys. Rev. Lett.*, **56**, 930 (1986).
3. J. E. Stern, B. D. Terris, H. J. Mamin, and D. Rugar, *Appl. Phys. Lett.*, **53**, 2717 (1988).
4. Y. Martin and K. K. Wickramasinghe, *Appl. Phys. Lett.*, **50**, 1455 (1987).
5. U. Hermann, *J. Vac. Sci. Technol.*, **B9**, 465 (1991).
6. Y. Martin, C. C. Williams, and H. K. Wickramasinghe, *J. Appl. Phys.*, **61**, 4723 (1987).
7. G. M. McClelland, R. Erlandsson, and S. Chiang, "Review of Progress in Quantitative Nondestructive Evaluation", edited by D. O. Thompson and D. E. Cimenti, Plenum, New York 1987, Vol. 6B, p. 1307.
8. A. L. Weisenborn, R. K. Hansma, T. R. Albrecht, and C. F. Quate, *Appl. Phy. Lett.*, **54**, 2651(1989).
9. J. N. Israelachevili, "Intermolecular and Surfaces", Academic, London 1985.
10. D. Sarid, "Scanning Force Microscopy", Oxford University, New York 1991.
11. D. Sarid and V. Elings, *J. Vac. Sci. Technol.*, **B9**, 431 (1991).
12. For example : J. Vac. Sci. Technol., **B9(2)**, part II, "*Microelectronics and nanometer structures*" (1991).
13. P. K. Hansma and J. Tersoff, *J. Appl. Phys.*, **61**, R1 (1987).
14. G. Binnig, H. Rohrer, Ch. Gerber, and E. Weibel, *Phys. Rev. Lett.*, **49**, 57 (1982).
15. G. Binnig and D. P. E. Smith, *Rev. Sci. Instrum.*, **57**, 1688 (1986).
16. B. Drake, C. B. Prater, A. L. Weisenhorn, S. A. C. Gould, D. S. Cannell, H. G. Hansma, P. K. Hansma, T. R. Albrecht, and C. F. Quate, *Science*, **243**, 1586 (1989).
17. R. H. Good, Jr. and E. W. Muller, "Encyclopedia of Physics", Springer, Berlin 1956, **21** 176.
18. M. Fotino, *Proceed. Electr. Micro. Soc. Am.*, **49**, 386

(1991).
19. A. J. Melmed, *J. Vac. Sci. Technol.*, **B9**, 601 (1991).
20. M. J. Heben, M. M. Dovek, N. S. Lewis, R. M. Penner, and C. F. Quate, *J. Microsc.*, **152**, 651 (1988).
21. M. J. Heben, R. M. Penner, N. S. Lewis, M. M. Dovek, and C. F. Quate, *Appl. Phys. Lett.*, **54**, 1421 (1989).
22. *Physics Today*, Jan., 80 (1992).
23. R. Yang, K. M. Dalsin, D. F. Evans, L. Christensen, and W. A. Hendeickson, *J. Phys. Chem.*, **93**, 511 (1989).
24. R. Yang, D. F. Evans, L. Christensen, and W. A. Hendeickson, *J. Phys. Chem.*, **94**, 6117 (1990).
25. W. M. Hecki and D. P. E. Smith, *J. Vac. Sci. Technol.*, **B9**, 1159 (1991).
26. G. L. Vandentop, P. A. P. Nascente, M. Kawasaki, D. F. Ogletree, G. A. Somorjai and M. Salmeron, *J. Vac. Sci. Technol.*, **B9**, 2273 (1991).
27. K. F. Turner, Y. M. LeGrice, B. R. Stoner, J. T. Glass, and R. J. Nemanich, *J. Vac. Sci. Technol.*, **B9**, 914 (1991).
28. J. Colchero, O. Marti, J. Mlynek, A. Humbert, C. R. Henny, and C. Chapon, *J. Vac. Sci. Technol.*, **B9**, 794 (1991).
29. A. Brodde, G. Wilhelmi, D. Badt, H. Wengelnik, and H. Neddermyer, *J. Vac. Sci. Technol.*, **B9**, 920 (1991).
30. M. O. Waranabe, T. Kuroda, K. Tanaka, and A. Sakai, *J. Vac. Sci. Technol.*, **B9**, 924 (1991).
31. D. D. Chamoliss and R. J. Wilson, *J. Vac. Sci. Technol.*, **B9**, 928 (1991).
32. G. Caple, B. L. Wheeler, R. Swift, T. L. Porter, and S. Jeffers, *J. Phys. Chem.*, **94**, 3059 (1990).
33. D. Jeon, J. Kim, M. C. Gallagher, R. F. Wills, and Y.-T. Kim, *J. Vac. Sci. Technol.*, **B9**, 1154 (1991).
34. T. L. Porter, C. Y. Lee, B. L. Wheeler, and G. Caple, *J. Vac. Sci. Technol.*, **A9**, 1452 (1991).
35. Y. Oka and A. Takahashi, *Polym. J.* **23**, 805 (1991).
36. S. Kempf, H. W. Rotter, S. N. Magonov, W. Gronski, and H.-J. Cantow, *Polym. Bull.*, **24**, 325 (1990).
37. G. Lee, P. G. Arscott, V. A. Bloomfield, D. F. Evans, *Science*, **244**, 475 (1989).
38. P. G. Arscott, G. Lee, V. A. Bloomfield, D. F. Evans, *Nature*, **339**, 485 (1989).
39. D. D. Dunlap and C. Bustamante, *Nature*, **342**, 204 (1989).
40. D. C. Dahn, M. O. Watanabe, B. L. Blackford, M. H. Jericho, and T. J. Beveridge, *J. Vac. Sci. Technol.*, **A6**, 548 (1988).
41. T. J. McMaster, H. J. Caar, M. J. Miles, P. Cairns, and V. J. Morris, *Macromolecules*, **24**, 1428 (1991).
42. R. D. Edstrom, M. H. Meinke, M. H. Yang, X. R. Yang, and D. F. Evans, *Biochemistry*, **28**, 939 (1989).
43. J. P. Rabe and S. Buchholz, *Makromol. Chem., Makromol. Symp.*, **50**, 261 (1991).
44. B. Michel, G. Travaglini, H. Roher, C. Joachim, and M. Amrein, *Z. Phys.* **B-76**, 99 (1989).
45. D. P. E. Smith, J. K. H. Horber, G. Binning, and H. Nejoh, *Nature*, **344**, 641 (1990).
46. R. Yang, X. R. Yang, D. F. Evans, W. A. Hendrickson, and J. Baker, *J. Phys. Chem.*, **94**, 6123 (1990).
47. D. Reneker, J. Schnier, B. Howell, and H. Harary, *Polym. Commun.*, **31**, 167 (1990).
48. J. Petermann, *Bull. Inst. Chem. Res., Kyoto Univ.*, **69**, 84 (1991).
49. J. P. Rabe, M. Sano, D. Batchelder, and A. A. Kalatchev, *J. Micros.* **152**, 573 (1988).
50. H. Fuchs, L. M. Eng, R. Sander, J. Petermann, K. D. Jandt, and T. Hoffmann, *Polym. Bull.*, **26**, 95 (1991).
51. H. S. Mizes, J. S. Foster, *Science*, **244**, 599 (1989).
52. H. Birk, J. Glatz-Reichenbach, Li-Jie, E. Schreck, and K. Dransfeld, *J. Vac. Sci. Technol.* **B9**, 1162 (1991).
53. J. Glatz-Reichenbach, Li-Jie, D. Schilling, E. Schreck, and K. Dransfeld, *Ferroelectrics*, **109**, 309 (1990).
54. T. Furukawa, *IEEE Trans. Electr. Insul.*, **EI-24**, 375 (1985).
55. D. A. Bonnell and M. Angelopoulos, *Synth. Met.*, **33**, 301 (1989).
56. M. A. McCord and R. F. W. Peace, *J. Vac. Sci. Technol.*, **B4**, 86 (1986).
57. M. A. McCord and R. F. W. Peace, *J. Vac. Sci. Technol.*, **B6**, 293 (1988).

58. M. H. Zhang, L. S. Hordon, S. W. J. Kuan, P. Maccagno, and R. F. W. Peace, *J. Vac. Sci. Technol.*, **B7**, 1717 (1989).
59. A. L. Weisenhorn, P. K. Hansma, C. F. Quate, *J. Appl. Phys.* **54**, 2651 (1989).
60. S. Manne, P. K. Hansma, J. Massie, V. B. Elings, A. A. Gewirth, *Science*, **251**, 183 (1991).
61. R. Patil, S. -J. Kim, E. Smith, D. H. Reneker, and A. L. Weisenhorn, *Polym. Commun.*, **31**, 455 (1990).
62. P. H. Geil and D. H. Reneker, *J. Polym. Sci.*, **51**, 569 (1961).
63. S. N. Magonov, K. Qvarnstrom, V. Elings, and H. -J. Cantow. *Polym. Bull.*, **25**, 689 (1991).
64. W. Stocker, G. Bar, M. Kunz, M. Moller, S. N. Magonov, and H. -J. Cantow, *Polym. Bull.*, **26**, 215 (1991).
65. S. N. Magonov, G. Bar, H. -J. Cantow, H. -D. Bauer, and M. Schwoerer, *Polym. Bull.*, **26**, 223 (1991).
66. B. Lotz, J. C. Wittmann, W. Stocker, S. N. Magonov, and H. -J. Cantow, *Polym. Bull.*, **26**, 209 (1991).
67. S. N. Magonov, S. Kempf, M. Kimming, and H. -J. Cantow. *Polym. Bull.*, **26**, 715 (1991).
68. For example : K. J. Ihn, M. Tsuji, S. Isoda, A. Kawaguchi, K. Katayama, Y. Tanaka, and H. Sato, *Macromolecules*, **23**, 1781 (1990).
69. E. J. Keller, *J. Appl. Crystalogr.*, **22**, 19 (1989).
70. K. J. Ihn, P. Dietz, F. Motamedi, D. Fenwick, J. C. Wittmann, P. K. Hansma, and P. Smith, *in preparation*.
71. J. C. Wittmann and P. Smith, *Nature*, **352**, 414 (1991).
72. H. Hansma, F. Motamedi, J. C. Wittmann, P. Smith, and P. K. Hansma, *Polym. Bull.*, to be published (1992).
73. D. Fenwick, K. J. Ihn, F. Motamedi, J. C. Wittmann, and P. Smith, *in preparation*.
74. C. Park, K. -S. Park, Y. -S. Huh, I. C. Jeon. S. Kim, *J. Vac. Sci. Technol.*, **B9**, 636 (1991).
75. T. Kato, F. Osaka, I. Tanaka, and S. Ohkouchi, *J. Vac. Sci. Technol.*, **B9**, 1981 (1991).
76. W. K. Lo and J. C. H. Spence, *Proceed. Electr. Micro. Soc. Am.*, **49**, 384 (1991).
77. V. S. Edel'man, A. M. Troyanovskii, M. S. Khaikin, G. A. Stepanyan, and A. P. Volodin, *J. Vac. Sci. Technol.*, **B9**, 618 (1991).
78. S. Chiang, D. D. Chambliss, V. M. Hallmark, R. J. Wilson, J. K. Brown, and Cj. Woll, *Proceed. Electr. Micro. Soc. Am.*, **49**, 370 (1991).
79. K. A. Fisher, M. G. L. Gustaffsson, M. B. Shattuck, and J. Clarke, *Proceed. Electr. Micro. Soc. Am.*, **49**, 54 (1991).
80. J. Harris, A. Partridge, J. Partridge, and R. Nielsen, *Proceed. Electr. Micro. Soc. Am.*, **49**, 388 (1991).
81. J. A. N. Zasadzinski, J. Schneir, J. Gurley, V. Elings, and P. K. Hansma, *Science*, **239**, 1013 (1988).
82. J. A. N. Zasadzinski and S. M. Bailey, *J. Electron. Microsc. Tech.*, **13**, 309 (1989).
83. J. T. Woodward, J. A. N. Zasadzinski, and P. K. Hansma, *J. Vac. Sci. Technol.*, **B9**, 1231 (1991).
84. I. Fujiwara, C. Ishimoto, and J. Seto., *J. Vac. Sci. Technol.*, **B9**, 1148 (1991).
85. H. G. Hansma, S. A. C. Gould, P. K. Hansma, H. E. Gaub, M. L. Longo, and J. A. N. Zasadzinski, *Langmuir*, **7**, 1051 (1991).
86. C. R. Clemmer and T. P. Beebe, *Science*, **251**, 640 (1991).
87. O. M. Leung and M. C. Goh, *Science*, **255**, 64 (1992).
88. T. J. McMaster, H. J. Carr, M. J. Miles, P. Cairns, and V. J. Morris, *Macromolecules*, **24**, 1428 (1991).